*photonics*

MDPI

*Communication*

# Photonic-Assisted Microwave Frequency Measurement Using High Q-Factor Microdisk with High Accuracy

**Mengyao Zhao [1], Wenyu Wang [1], Lei Shi [1], Chicheng Che [2] and Jianji Dong [1,3,*]**

[1] Wuhan National Laboratory for Optoelectronics, Huazhong University of Science and Technology, Wuhan 430074, China
[2] Huazhong Institute of Electro-Optics—Wuhan National Laboratory for Optoelectronics, Wuhan 430223, China
[3] Optics Valley Laboratory, Wuhan 430074, China
* Correspondence: jjdong@hust.edu.cn

**Abstract:** Frequency measurement plays a crucial role in radar, communication, and various applications. The photonic-assisted frequency measurement method offers several advantages, including resistance to electromagnetic interference, broad bandwidth, and low power consumption. Notably, frequency-to-time mapping enables the measurement of various microwave signal types, such as single-frequency, multiple-frequency, frequency hopping, and chirped signals. However, the accuracy of this method is currently limited due to the absence of resonant devices with high-quality factors, which are essential for achieving higher-precision measurements. In this work, a frequency measurement method based on an ultrahigh-quality-factor microdisk is proposed. By establishing a correlation between the time difference and the frequency to be measured, a reduction in measurement error to below 10 MHz within a frequency measurement range of 3 GHz is realized. Our work introduces a new approach to frequency measurement using optical devices, opening new possibilities in this field.

**Keywords:** microwave frequency measurement; microwave photonics; microdisk



**Citation:** Zhao, M.; Wang, W.; Shi, L.; Che, C.; Dong, J. Photonic-Assisted Microwave Frequency Measurement Using High Q-Factor Microdisk with High Accuracy. *Photonics* **2023**, *10*, 847. https://doi.org/10.3390/photonics10070847

Received: 29 June 2023
Revised: 19 July 2023
Accepted: 20 July 2023
Published: 21 July 2023



## 1. Introduction

In applications involving microwave signals such as wireless communications [1], astronomy [2] and materials [3], it is a fundamental requirement to accurately determine the frequency of detected microwave signals [1,4]. Conventional frequency measurement methods in the electrical domain face challenges in identifying high-frequency microwave signals and are susceptible to electromagnetic interference. Microwave photonics (MWP) uses optical signal as the carrier for processing radio frequency (RF) signals. When combined with optical devices, MWP can also offer outstanding performances, including expanded bandwidth, compact size, light weight, and low loss [5–8].

Two main principles of optical microwave frequency measurement are widely employed: frequency-to-power mapping (FTPM) [9–12] and frequency-to-time mapping (FTTM) [13–17]. FTPM enables instantaneous frequency measurement (IFM) by establishing the relationship between system output power and microwave frequency. By detecting the system output power, the previously unknown microwave signal frequency can be determined. Integrated structures such as Bragg gratings [18], the microring resonator (MRR) [19–21], the Mach–Zehnder interferometer (MZI) [22] and microdisks [23,24] have been employed to implement FTPM. FTTM focuses on establishing the relationship between microwave frequency and time. Although FTTM does not support IFM, it has the potential to use statistical results to obtain the frequencies of many types of microwave signals, including single-frequency, multi-frequency, frequency-hopping and chirped signals. FTTM has been implemented with structures such as MRR [25,26], the stimulated Brillouin scattering (SBS) effect [27–31], Fourier domain mode locked optoelectronic oscillator

(OEO) [32] and dispersive medium [33]. However, some of these approaches introduce nonlinear effects and increase system complexity, while others are limited by low-quality factor resonant devices, resulting in measurement errors in the tens or hundreds of megahertz. Considering the increasing demands for high-speed information transmission and precise frequency analysis, there remains a critical need to develop a frequency identification system with reduced measurement error.

In this paper, we propose a microwave frequency measurement system using a whispering-gallery-mode (WGM) magnesium fluoride microdisk resonator. Through experimental demonstrations, we show that the microdisk possesses an exceptional quality factor (Q-factor) exceeding $10^8$, allowing the system to achieve a low single-frequency measurement error of less than 10 MHz within the frequency range of 3 GHz.

## 2. Principle

Figure 1a illustrates the schematic diagram of our proposed frequency measurement system. The five images in Figure 1b show the expected waveforms at different points in the system. An arbitrary waveform generator (AWG) generates a triangular wave signal which is then supplied to a tunable laser source (TLS). Driven by the triangular waveform, the output frequency of the tunable laser source, denoted as $f_c$, is synchronized, and it periodically scans at about 1550 nm. Meanwhile, the unknown RF signal, denoted as $f_m$, is fed into the intensity modulator (IM), and the carrier-suppressed modulated signal is obtained by adjusting the bias voltage of the modulator. Subsequently, a bandpass filter (BPF) selectively filters one of the sidebands, as shown in Figure 1b, retaining only the upper sideband frequency ($f_c + f_m$). Then, the filtered light is directed into a microdisk with high Q-factor, and a photodetector (PD) is used to detect the output light at the through-port of the microdisk. Finally, an oscilloscope (OSC) displays the electric signals collected by the PD. Since the signal is detected from the through-port of the microdisk, a dip will appear on the OSC when the input optical frequency is exactly equal to one of the resonant frequencies of the microdisk.

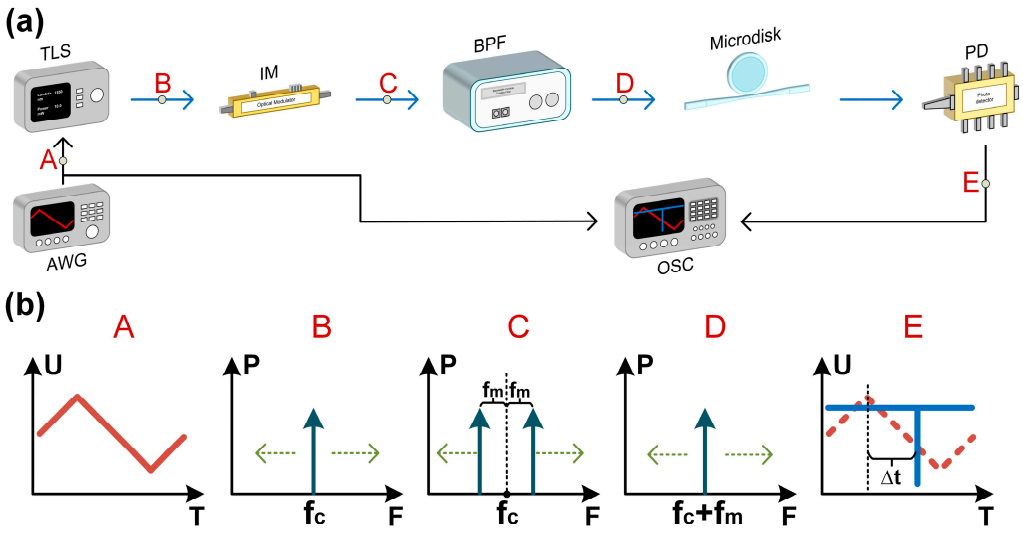


**Figure 1.** (**a**) Schematic diagram of the frequency measurement principle. The blue lines indicate the transmission path of the optical signal, and the black lines indicate the transmission path of the electric signal. AWG, arbitrary waveform generator; TLS, tunable laser source; IM, intensity modulator; BPF, bandpass filter; PD, photodetector; OSC, oscilloscope. (**b**) The corresponding waveform or spectrum diagram at points A, B, C, D and E marked in the schematic diagram.

There will be a time difference Δt between the occurrence of the dip and the beginning of the falling edge of the triangular wave emitted by AWG, as illustrated in the waveform at point E in Figure 1b. When $f_m$ varies, during the frequency scanning of $f_c$, the timing at which ($f_c + f_m$) matches the resonant wavelength of the microdisk also changes, conse-

quently leading to a variation in Δt. As Δt is generated after the light passes through the entire system, the time delay caused by all the devices in the system has been included. Given the linear frequency sweep of the TLS, the fitting relationship can be expressed as:

$$f_{\text{unknown}} = a \cdot (\Delta t) + b. \quad (1)$$

Here, $f_{\text{unknown}}$ represents the unknown frequency of the microwave signal, while $a$ and $b$ are constants determined by the practical system. When the relationship of Equation (1) is established, the unknown microwave frequency can be identified by measuring Δt. Consequently, we can successfully measure the frequency of the microwave signal through this approach.

## 3. Results

First, we characterize the basic parameters of the microdisk. Figure 2a presents the microdisk utilized in this experiment, with a diameter of 8 mm and a thickness of 0.5 mm. By using the ultra-smooth toroidal boundary surface, the light field is confined in a very small space, and the high-order modes are suppressed to achieve ultra-low loss resonance, and the WGM microdisk with an ultra-high Q factor and minimal mode volume is obtained. The employed TLS exhibits a proportional relationship between the applied peak-to-peak voltage and the sweep frequency range. To measure the free spectral range (FSR) of the microdisk, a triangular wave with a peak-to-peak voltage of 5.143 V and a frequency of 50 Hz is applied. This allows the TLS to periodically sweep across the frequency range of 30 GHz, centered around 1550 nm, with a period of 20 ms. The waveform captured from the through-port of the microdisk, as detected by the PD, is depicted in Figure 2b, exhibiting an FSR of approximate 10 GHz. Figure 2c shows the resonant mode we selected for frequency measurement, which demonstrated a 3 dB bandwidth of 0.6291 MHz at a wavelength of 1556.77 nm. This implies a loaded Q-factor of $3.06 \times 10^8$ for the microdisk.

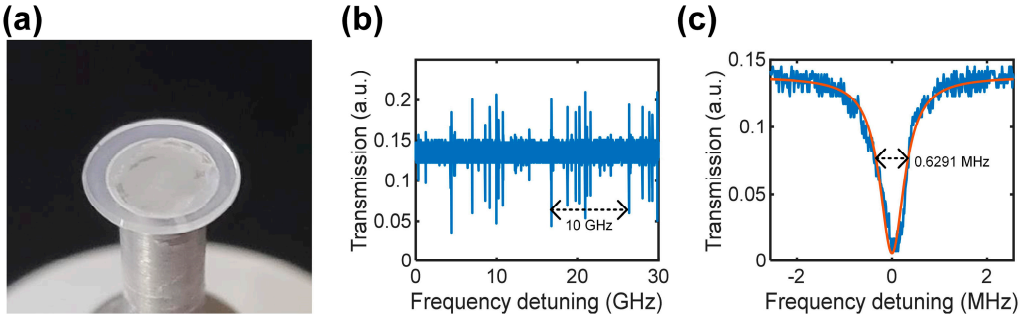


**Figure 2.** (**a**) Microdisk used in the experiment. (**b**) TLS sweeps in the 30 GHz frequency range to determine the FSR of the microdisk. The measured FSR is approximately 10 GHz. (**c**) The resonant mode selected for frequency measurement.

The experimental setup of the microwave frequency measurement is presented in Figure 3. The speed and range of the sweep frequency of the TLS (New Focus: Tunable Laser Controller TLB-6700 and External Cavity Diode Laser TLB-6730P) are determined using a triangular wave generated by the AWG (Agilent 33250A). To measure the microwave signal frequency, the parameters of the triangular wave are configured with a peak-to-peak value of 0.857 V and a frequency of 32 Hz, resulting in a sweep frequency range of 5 GHz and a period of 31.25 ms for the TLS. Subsequently, the TLS generates a frequency-swept optical carrier at a power of 10 mW, with a central wavelength close to 1556.77 nm. An isolator is placed after the TLS to safeguard the light source. To amplify the optical carrier, an erbium-doped fiber amplifier (EDFA) is employed, with an output optical power of 15 dBm. A polarization controller (PC) adjusts the polarization state of the incoming light to achieve the maximum modulation efficiency of IM (JDS Uniphase 21049397, the half-wave voltage is 5.9 V). The RF signal generated by a waveform generator (SinoLink Technologies

SLFS24C) is fed into the IM, with a power of 18 dBm. Simultaneously, the bias voltage of the IM is set as 2.27 V by a direct-current voltage source (HAMEG HMP4040), enabling the suppression of the optical carrier. Afterwards, a BPF (Alnair Labs BVF-300CL) is used to eliminate the lower sideband, ensuring that the light entering the microdisk contains only the upper sideband. An additional EDFA is applied to compensate for the insertion loss of the BPF, and the optical power is controlled to about 13 dBm by an attenuator (ATT) before entering the microdisk. A PD (THORLABS PDA05CF2) is used to detect light signals. Finally, a PC is adjusted until clear resonant dips become visible on the OSC (Agilent Technologies DSO7054A), indicating successful coupling with the microdisk. The coupling of the optical microdisk is accomplished using a tapered fiber. By moving the edge of the microdisk along the tapered fiber and achieving coupling at the appropriate position on the fiber diameter, the excitation of high-order modes can be minimized, resulting in a clear spectrum.

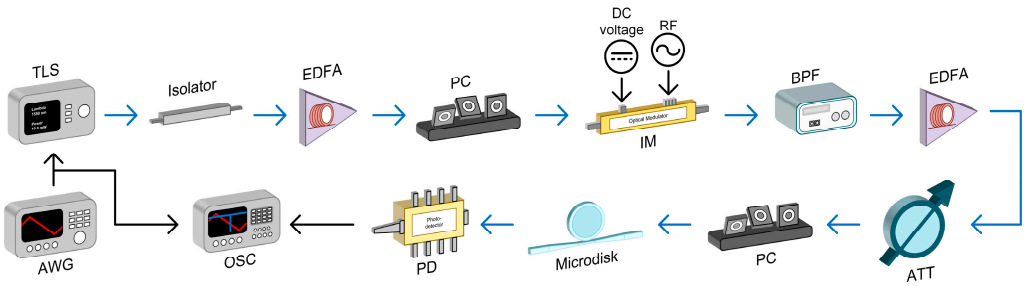


**Figure 3.** Experimental setup of the microwave frequency measurement. AWG, arbitrary waveform generator; TLS, tunable laser source; EDFA, erbium-doped fiber amplifier; PC, polarization controller; IM, intensity modulator; DC voltage, direct-current voltage; RF, radio frequency; BPF, bandpass filter; ATT, attenuator; PD, photodetector; OSC, oscilloscope.

Then, Figure 4a illustrates the linear relationship between Δt and the microwave frequency. We select 13 points between 14.25 and 17.25 GHz with equal frequency intervals of 0.25 GHz to establish this relationship and obtain $a$ = 0.3527 and $b$ = 11.8363. With this relationship, once Δt is tested, it can be brought into Equation (1), thus determining the previously unknown RF frequency. Figure 4b presents the calculated frequency measurement error within the range of 14.25 to 17.25 GHz. Error points fall between the two orange dotted lines, indicating that the error remains below 10 MHz throughout the tested frequency range of 3 GHz.

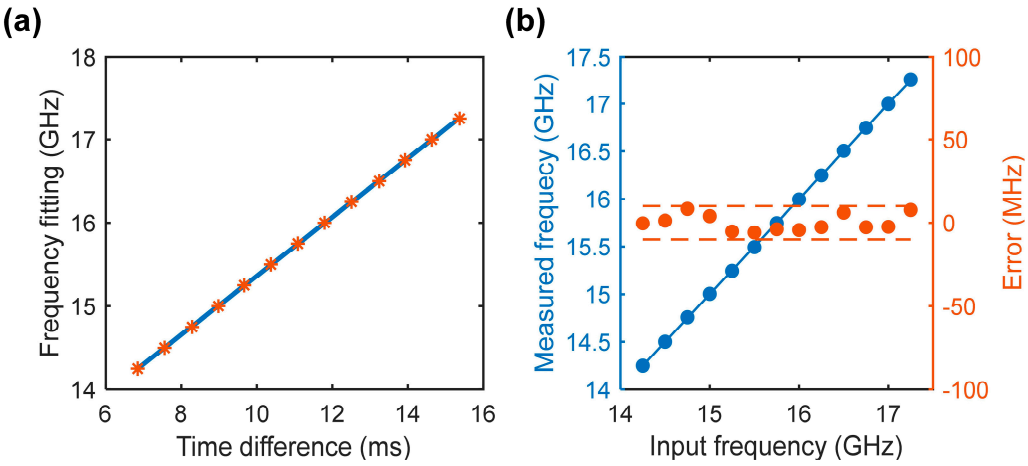


**Figure 4.** (**a**) Fitting relationship between time difference and microwave frequency. (**b**) Frequency (blue dots) and corresponding error (orange dots) obtained by the experiment. The error between two orange dashed lines indicates an error of less than 10 MHz.

The root mean square error $\alpha$ is defined by:

$$\alpha = \sqrt{\frac{\Sigma_{i=1}^{N}[f_t(i) - f_m(i)]^2}{N}}. \quad (2)$$

Here, $f_t(i)$ and $f_m(i)$ are the tested and real RF frequencies, respectively. $N$, representing the number of statistical data points, is 13 based on the data presented in Figure 4. By applying Equation (2) to our experimental results, the calculated value of $\alpha$ is 4.8033 MHz.

Next, according to the fitted frequency range, we evaluate the function of the system with some arbitrary frequency microwave signals. Figure 5 shows the results obtained when loading microwave signals with frequencies of 14.8 GHz, 15.1 GHz, 15.6 GHz, and 16.1 GHz into IM. The measured $\Delta$t values corresponding to these frequencies are 8.4226 ms, 9.2486 ms, 10.6650 ms and 12.0961 ms, respectively. By referring to the fitting relationship in Figure 4a, we determine the actual test frequencies to be 14.8066 GHz, 15.0979 GHz, 15.5974 GHz, and 16.1021 GHz. The measurement errors of these four frequencies are all below 10 MHz. These results show the successful realization of the expected functionality of the proposed system.

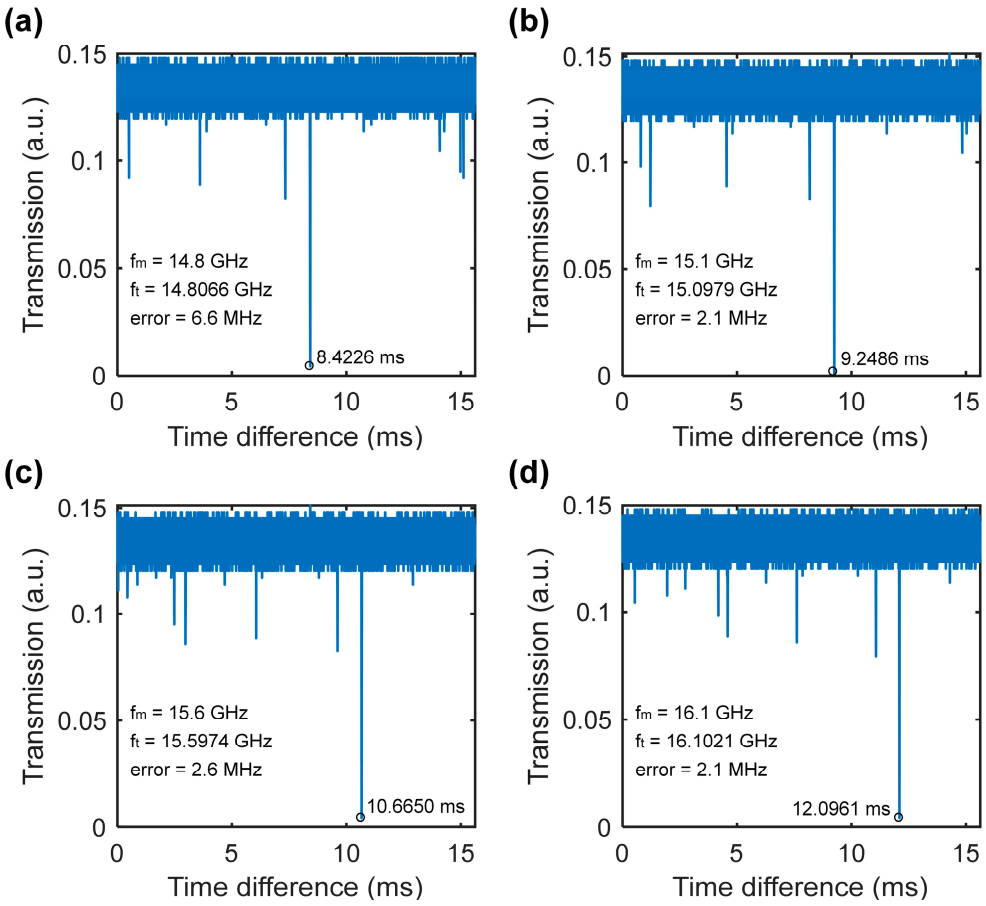


**Figure 5.** Verification of system functions. The input RF frequencies to be measured ($f_m$) are (**a**) 14.8 GHz, (**b**) 15.1 GHz, (**c**) 15.6 GHz, and (**d**) 16.1 GHz, and the frequencies tested by experiment ($f_t$) are 14.8066 GHz, 15.0979 GHz, 15.5974 GHz, and 16.1021 GHz, respectively.

During the experiments, we observed that the extinction ratio of the selected resonant mode used for frequency measurement varies with changes in the RF signal power input to the IM. The blue circles in Figure 6 are tested data points, and the orange curve is a polynomial fitting curve of the relationship between the RF power and extinction ratio. With this correspondence, an estimate of the RF power can be obtained by calculating the extinction ratio of the resonant mode. In order to explain the above phenomenon, we

observe with an optical spectrum analyzer (DEVISER AE8600) that as the power of the RF signal input to IM decreases, the floor noise of the optical signal after IM modulation increases, and the power difference between the sideband and the floor noise decreases.

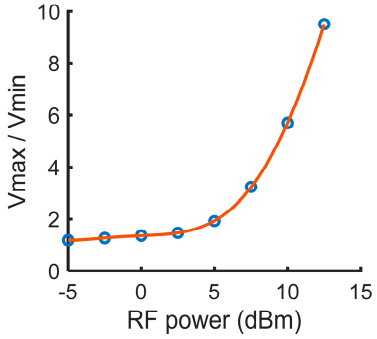


**Figure 6.** Measured extinction ratio of resonant mode of a 12.5 GHz microwave signal.

## 4. Discussion

In Table 1, we compare the results obtained from existing works in the field of microwave photonics that utilize similar principles for frequency measurement.

**Table 1.** Comparison of existing optically assisted microwave frequency measurement results.

| Structure | Range (GHz) | Error (MHz) | Reference |
|---|---|---|---|
| Silicon MRR | 14–25 | 200 | [34] |
| InP MZI | 5–15 | 200 (rms) * | [22] |
| TriPleX MRR | 0.5–4 | 93.6 (rms) | [20] |
| Silicon Microdisk | 1.6–40 | 60 | [24] |
| Silicon MRR | 3–19 | 500 | [21] |
| Silicon MRR | 1–30 | 237.3 (rms) | [25] |
| Silicon waveguide Bragg grating | 0–32 | 773 (rms) | [18] |
| Magnesium fluoride microdisk | 14.25–17.25 | 10 | This work |

* "rms" means root mean square.

From the comparison in Table 1, we can see that the frequency measurement system proposed in this paper achieves high measurement accuracy in a single frequency identification process, reducing both the existing frequency measurement error and the root mean square of the error by an order of magnitude. Additionally, the measurement error can be further reduced by choosing a resonant mode with a higher Q-factor. For a Q-factor of $10^8$ selected in this paper, the corresponding frequency measurement accuracy is in the order of 0~10 MHz, and a one-order-of-magnitude increase in the Q-factor of the resonator corresponds to a one-order-of-magnitude decrease in the theoretical frequency measurement error. A TLS with higher frequency sweep linearity can be selected to reduce the nonlinear errors caused by nonlinear sweep frequency. Furthermore, the frequency measurement range of our work can be extended through different approaches. One approach is to optimize the coupling between the tapered fiber and the microdisk to minimize the excitation of higher-order modes. So, the FSR of the microdisk, which is approximately 10 GHz in our experiment, can be utilized to achieve a larger frequency measurement range in a single measurement process. Another method is to re-calibrate the linear relationship between $\Delta t$ and the frequency to be measured whenever the RF range is changed. This allows for flexibility in adapting to different frequency ranges. The minimum value of the frequency range achievable by this method depends on the linewidth of the single-frequency laser used in the system. A narrower linewidth ensures better isolation of the modulation sidebands when the IM is driven by low-frequency microwave signals. Once a modulation sideband can be separated, frequency measurement can be achieved by this method. The maximum value of the frequency range depends on the frequency response characteristics of the devices used in the system. For instance, the maximum microwave

frequency supported by the IM and PD determines the upper limit of the frequency measurement range. By employing devices with wider frequency response capabilities, a larger maximum frequency measurement range can be achieved.

## 5. Conclusions

In summary, we propose a simple and efficient method for the high-precision identification of microwave signal frequencies. The experimental results confirm that the proposed method achieves an error of less than 10 MHz within the frequency range of 14.25~17.25 GHz. If combined with subsequent packaging, it can provide a solution for realizing a high-quality microwave frequency measurement system with small size and low weight. Integrating the microdisk, tapered fiber, IM, light source, and photodetector together in a single package will also improve the stability of the system. By implementing optimization techniques such as improved coupling, recalibration, and selecting high-Q-factor resonant modes, the measurement range and accuracy can be further enhanced to meet the specific requirements of various applications. The findings of this study contribute to advancing the field of microwave frequency measurement and offer practical applications in radar, wireless communications, and related fields.

**Author Contributions:** Conceptualization, M.Z.; methodology, M.Z.; resources, L.S., C.C. and J.D.; data curation, M.Z. and W.W.; writing—original draft preparation, M.Z.; writing—review and editing, J.D.; supervision, J.D.; funding acquisition, J.D. All authors have read and agreed to the published version of the manuscript.

**Funding:** The National Natural Science Foundation of China (62075075, 62275088, U21A20511) and the Innovation Project of Optics Valley Laboratory (Grant No. OVL2021BG001).

**Institutional Review Board Statement:** Not applicable.

**Informed Consent Statement:** Not applicable.

**Data Availability Statement:** The data that support the findings of this study are available from the corresponding author upon reasonable request.

**Conflicts of Interest:** The authors declare no conflict of interest.

## References

1. Domdouzis, K.; Kumar, B.; Anumba, C. Radio-Frequency Identification (RFID) applications: A brief introduction. *Adv. Eng. Inform.* **2007**, *21*, 350–355. [CrossRef]
2. Bolton, S.J.; Levin, S.M.; Guillot, T.; Li, C.; Kaspi, Y.; Orton, G.; Wong, M.H.; Oyafuso, F.; Allison, M.; Arballo, J.; et al. Microwave observations reveal the deep extent and structure of Jupiter's atmospheric vortices. *Science* **2021**, *374*, 968–972. [CrossRef]
3. Ali, L.; Wang, C.; Meng, F.Y.; Wei, Y.C.; Tan, X.; Adhikari, K.K.; Zhao, M. Simultaneous measurement of thickness and permittivity using microwave resonator-based planar sensor. *Int. J. RF Microw. Comput. Aided Eng.* **2021**, *31*, e22794. [CrossRef]
4. Marpaung, D.; Roeloffzen, C.; Heideman, R.; Leinse, A.; Sales, S.; Capmany, J. Integrated microwave photonics. *Laser Photonics Rev.* **2013**, *7*, 506–538. [CrossRef]
5. Zou, X.; Lu, B.; Pan, W.; Yan, L.; Stöhr, A.; Yao, J. Photonics for microwave measurements. *Laser Photonics Rev.* **2016**, *10*, 711–734. [CrossRef]
6. Pan, S.; Yao, J. Photonics-Based Broadband Microwave Measurement. *J. Light. Technol.* **2017**, *35*, 3498–3513. [CrossRef]
7. Capmany, J.; Novak, D. Microwave photonics combines two worlds. *Nat. Photonics* **2007**, *1*, 319–330. [CrossRef]
8. Pelusi, M.; Luan, F.; Vo, T.D.; Lamont, M.R.E.; Madden, S.J.; Bulla, D.A.; Choi, D.-Y.; Luther-Davies, B.; Eggleton, B.J. Photonic-chip-based radio-frequency spectrum analyser with terahertz bandwidth. *Nat. Photonics* **2009**, *3*, 139–143. [CrossRef]
9. Zhu, Y.-L.; Wu, B.-L.; Li, J.; Wang, M.-G.; Xiao, S.-Y.; Yan, F.-P. Switchable instantaneous frequency measurement by optical power monitoring based on DP-QPSK modulator. *Chin. Phys. B* **2022**, *31*, 044202. [CrossRef]
10. Lin, T.; Zou, C.; Zhang, Z.; Zhao, S.; Liu, J.; Li, J.; Zhang, K.; Yu, W.; Wang, J.; Jiang, W. Differentiator-Based Photonic Instantaneous Frequency Measurement for Radar Warning Receiver. *J. Light. Technol.* **2020**, *38*, 3942–3949. [CrossRef]
11. Emami, H.; Sarkhosh, N.; Ashourian, M. Reconfigurable photonic radar warning receiver based on cascaded grating. *Opt. Express* **2013**, *21*, 7734–7739. [CrossRef]
12. Emami, H.; Sarkhosh, N.; Ashourian, M. Photonic simultaneous frequency identification of radio-frequency signals with multiple tones. *Appl. Opt.* **2013**, *52*, 5508–5515. [CrossRef]
13. Nguyen, T.A.; Chan, E.H.W.; Minasian, R.A. Photonic Multiple Frequency Measurement Using a Frequency Shifting Recirculating Delay Line Structure. *J. Light. Technol.* **2014**, *32*, 3831–3838. [CrossRef]

14. Nguyen, T.A.; Chan, E.H.; Minasian, R.A. Instantaneous high-resolution multiple-frequency measurement system based on frequency-to-time mapping technique. *Opt. Lett.* **2014**, *39*, 2419–2422. [CrossRef] [PubMed]
15. Shi, J.; Zhang, F.; Ben, D.; Pan, S. Simultaneous Radar Detection and Frequency Measurement by Broadband Microwave Photonic Processing. *J. Light. Technol.* **2020**, *38*, 2171–2179. [CrossRef]
16. Zhou, Y.; Zhang, F.; Shi, J.; Pan, S. Deep neural network-assisted high-accuracy microwave instantaneous frequency measurement with a photonic scanning receiver. *Opt. Lett.* **2020**, *45*, 3038–3041. [CrossRef]
17. Shi, J.; Zhang, F.; Zhou, Y.; Pan, S.; Wang, Y.; Ben, D. Photonic scanning receiver for wide-range microwave frequency measurement by photonic frequency octupling and in-phase and quadrature mixing. *Opt. Lett.* **2020**, *45*, 5381–5384. [CrossRef]
18. Burla, M.; Wang, X.; Li, M.; Chrostowski, L.; Azana, J. Wideband dynamic microwave frequency identification system using a low-power ultracompact silicon photonic chip. *Nat. Commun.* **2016**, *7*, 13004. [CrossRef] [PubMed]
19. Yao, Y.; Zhao, Y.; Wei, Y.; Zhou, F.; Chen, D.; Zhang, Y.; Xiao, X.; Li, M.; Dong, J.; Yu, S.; et al. Highly Integrated Dual-Modality Microwave Frequency Identification System. *Laser Photonics Rev.* **2022**, *16*, 2200006. [CrossRef]
20. Marpaung, D. On-Chip Photonic-Assisted Instantaneous Microwave Frequency Measurement System. *IEEE Photonics Technol. Lett.* **2013**, *25*, 837–840. [CrossRef]
21. Zhu, B.; Zhang, W.; Pan, S.; Yao, J. High-Sensitivity Instantaneous Microwave Frequency Measurement Based on a Silicon Photonic Integrated Fano Resonator. *J. Light. Technol.* **2019**, *37*, 2527–2533. [CrossRef]
22. Fandino, J.S.; Munoz, P. Photonics-based microwave frequency measurement using a double-sideband suppressed-carrier modulation and an InP integrated ring-assisted Mach-Zehnder interferometer filter. *Opt. Lett.* **2013**, *38*, 4316–4319. [CrossRef]
23. Liu, L.; Jiang, F.; Yan, S.; Min, S.; He, M.; Gao, D.; Dong, J. Photonic measurement of microwave frequency using a silicon microdisk resonator. *Opt. Commun.* **2015**, *335*, 266–270. [CrossRef]
24. Chen, Y.; Zhang, W.; Liu, J.; Yao, J. On-chip two-step microwave frequency measurement with high accuracy and ultra-wide bandwidth using add-drop micro-disk resonators. *Opt. Lett.* **2019**, *44*, 2402–2405. [CrossRef]
25. Wang, X.; Zhou, F.; Gao, D.S.; Wei, Y.X.; Xiao, X.; Yu, S.H.; Dong, J.J.; Zhang, X.L. Wideband adaptive microwave frequency identification using an integrated silicon photonic scanning filter. *Photonics Res.* **2019**, *7*, 172–181. [CrossRef]
26. Zhou, F.; Chen, H.; Wang, X.; Zhou, L.; Dong, J.; Zhang, X. Photonic Multiple Microwave Frequency Measurement Based on Frequency-to-Time Mapping. *IEEE Photonics J.* **2018**, *10*, 1–7. [CrossRef]
27. Wang, H.; Dong, Y. High-performance transient SBS-based microwave measurement using high-chirp-rate modulation and advanced algorithms. *Opt. Lett.* **2023**, *48*, 3291–3294. [CrossRef]
28. Wang, H.; Dong, Y. Real-Time and High-Accuracy Microwave Frequency Identification Based on Ultra-Wideband Optical Chirp Chain Transient SBS Effect. *Laser Photonics Rev.* **2023**, *17*, 2200239. [CrossRef]
29. Liu, J.; Shi, T.; Chen, Y. High-Accuracy Multiple Microwave Frequency Measurement with Two-Step Accuracy Improvement Based on Stimulated Brillouin Scattering and Frequency-to-Time Mapping. *J. Light. Technol.* **2021**, *39*, 2023–2032. [CrossRef]
30. Jiang, H.; Marpaung, D.; Pagani, M.; Vu, K.; Choi, D.-Y.; Madden, S.J.; Yan, L.; Eggleton, B.J. Wide-range, high-precision multiple microwave frequency measurement using a chip-based photonic Brillouin filter. *Optica* **2016**, *3*, 30–34. [CrossRef]
31. Long, X.; Zou, W.; Chen, J. Broadband instantaneous frequency measurement based on stimulated Brillouin scattering. *Opt. Express* **2017**, *25*, 2206–2214. [CrossRef]
32. Hao, T.; Tang, J.; Shi, N.; Li, W.; Zhu, N.; Li, M. Multiple-frequency measurement based on a Fourier domain mode-locked optoelectronic oscillator operating around oscillation threshold. *Opt. Lett.* **2019**, *44*, 3062–3065. [CrossRef] [PubMed]
33. Nguyen, L. Microwave Photonic Technique for Frequency Measurement of Simultaneous Signals. *IEEE Photonics Technol. Lett.* **2009**, *21*, 642–644. [CrossRef]
34. Cao, R.; He, Y.; Zheng, R.; He, Z.; Zhi, Y.; Wang, X.; Zhang, J.; Yao, J. Microwave frequency measurement using a silicon integrated microring resonator. *Appl. Opt.* **2022**, *61*, 6671–6676. [CrossRef] [PubMed]